7. Thermoacoustics

Thermodynamic and fluid-dynamic processes in sound waves in gases can convert energy from one form to another. In these *thermoacoustic* processes [7.1, 2], high-temperature heat or chemical energy can be partially converted to acoustic power, acoustic power can produce heat, acoustic power can pump heat from a low temperature or to a high temperature, and acoustic power can be partially converted to chemical potential in the separation of gas mixtures. In some cases, the thermoacoustic perspective brings new insights to decades-old technologies. Well-engineered thermoacoustic devices using extremely intense sound approach the power conversion per unit volume and the efficiency of mature energy-conversion equipment such as internal combustion engines, and the simplicity of few or no moving parts drives the development of practical applications.

This chapter surveys thermoacoustic energy conversion, so the reader can understand how thermoacoustic devices work and can estimate some relevant numbers. After a brief history, an initial section defines vocabulary and establishes preliminary concepts, and subsequent sections explain engines, dissipation, refrigeration, and mixture separation. Combustion thermoacoustics is mentioned only briefly. Transduction and measurement systems that use heat-generated surface and bulk acoustic waves in solids are not discussed.

7.1 History

The history of thermoacoustic energy conversion has many interwoven roots, branches, and trunks. It is a complicated history because invention and technology development outside of the discipline of acoustics have sometimes preceded fundamental understanding; at other times, fundamental science has come first.

Rott [7.3, 4] developed the mathematics describing acoustic oscillations in a gas in a channel with an axial temperature gradient, with lateral channel dimensions of the order of the gas thermal penetration depth (typically ≈ 1 mm), this being much shorter than the wavelength (typically ≈ 1 m). The problem had been investigated by Rayleigh and by Kirchhoff, but without quantitative success. In Rott's time, the motivation to understand the problem arose largely from the cryogenic phenomenon known as Taconis oscillations – when a gas-filled tube is cooled from ambient temperature to a cryogenic temperature, the gas sometimes oscillates spontaneously, with large heat transport from ambient to the cryogenic environment. *Yazaki* [7.5] demonstrated convincingly that Rott's analysis of Taconis oscillations was quantitatively accurate.

A century earlier, *Rayleigh* [7.6] understood the qualitative features of such heat-driven oscillations: "If heat be given to the air at the moment of greatest condensation (i.e., greatest density) or be taken from it at the moment of greatest rarefaction, the vibration is encouraged." He had studied Sondhauss oscillations [7.7], the glassblowers' precursor to Taconis oscillations.

Applying Rott's mathematics to a situation where the temperature gradient along the channel was too weak to satisfy Rayleigh's criterion for spontaneous oscillations, *Hofler* [7.8] invented a standing-wave thermoacoustic refrigerator, and demonstrated [7.9] again that Rott's approach to acoustics in small channels was quantitatively accurate. In this type of refrigerator, the coupled oscillations of gas motion, temperature, and heat transfer in the sound wave are phased in time so that heat is absorbed from a load at a low temperature and waste heat is rejected to a sink at a higher temperature.

Meanwhile, completely independently, pulse-tube refrigeration was becoming the most actively investigated area of cryogenic refrigeration. This development began with *Gifford*'s [7.10] accidental discovery and subsequent investigation of the cooling associated with square-wave pulses of pressure applied to one end of a pipe that was closed at the other end. Although the relationship was not recognized at the time, this phenomenon shared much physics with Hofler's refrigerator. *Mikulin*'s [7.11] attempt at improvement in heat transfer in one part of this basic pulse-tube refrigerator led unexpectedly to a dramatic improvement of performance, and *Radebaugh* [7.12] realized that the resulting *orifice* pulse-tube refrigerator was in fact a variant of the Stirling cryocooler.

Development of Stirling engines and refrigerators started in the 19th century, the engines at first as an alternative to steam engines [7.13]. Crankshafts, multiple pistons, and other moving parts seemed at first to be essential. An important modern chapter in their development began in the 1970s with the invention of *free-piston* Stirling engines and refrigerators, in which each piston's motion is determined by interactions between the piston's dynamics and the gas's dynamics rather than by a crankshaft and connecting rod. Analysis of such complex, coupled phenomena is complicated, because the oscillating motion causes oscillating pressure differences while simultaneously the oscillating pressure differences cause oscillating motion. *Ceperley* [7.14,15] added an explicitly acoustic perspective to Stirling engines and refrigerators when he realized that the time phasing between pressure and motion oscillations in the heart of their regenerators is that of a traveling acoustic wave. Many years later, acoustic versions of such engines were demonstrated by *Yazaki* [7.16], *de-Blok* [7.17], and *Backhaus* [7.18], the last achieving a heat-to-acoustic energy efficiency comparable to that of other mature energy-conversion technologies.

7.2 Shared Concepts

7.2.1 Pressure and Velocity

For a monofrequency wave, oscillating variables can be represented with complex notation, such as

$$p(x,t) = p_{\mathrm{m}} + \mathrm{Re}\left[p_1(x)\mathrm{e}^{\mathrm{i}\omega t}\right] \tag{7.1}$$

for the pressure p, where p_{m} is the mean pressure, Re (z) indicates the real part of z, $\omega = 2\pi f$ is the angular frequency, f is the frequency, and the complex number p_1 specifies both the amplitude and the time phase of the oscillating part of the pressure. For propagation in the x direction through a cross-sectional area A in a duct, p_1 is a function of x. In the simple lossless, uniform-area situation the sinusoidal x dependence can be found from the wave equation, which can be written with $i\omega$ substituted for time derivatives as

$$\omega^2 p_1 + c^2 \frac{\mathrm{d}^2 p_1}{\mathrm{d}x^2} = 0\,, \tag{7.2}$$

where $c^2 = (\partial p/\partial\rho)_s$ is the square of the adiabatic sound speed, with ρ the density and s the entropy. In thermoacoustics, intuition is well served by thinking of (7.2) as two first-order differential equations coupling two variables, pressure p_1 and the x component of volume velocity, U_1:

$$\frac{\mathrm{d}p_1}{\mathrm{d}x} = -\frac{\mathrm{i}\omega\rho_{\mathrm{m}}}{A}U_1\,, \tag{7.3}$$

$$\frac{\mathrm{d}U_1}{\mathrm{d}x} = -\frac{\mathrm{i}\omega A}{\rho_{\mathrm{m}}c^2}p_1. \tag{7.4}$$

For a reasonably short length of duct Δx, these can be written approximately as

$$\Delta p_1 = -\mathrm{i}\omega L\, U_1\,, \tag{7.5}$$

$$p_1 = -\frac{1}{\mathrm{i}\omega C}\Delta U_1\,, \tag{7.6}$$

where

$$L = \frac{\rho_{\mathrm{m}}\Delta x}{A}\,, \tag{7.7}$$

$$C = \frac{A\Delta x}{\rho_{\mathrm{m}}c^2}\,. \tag{7.8}$$

Table 7.1 The acoustic–electric analog. The basic building blocks of thermoacoustic energy-conversion devices are inertances L, compliances C, viscous and thermal resistances R_{visc} and R_{therm}, gains (or losses) G, and power transducers

Acoustic variables	Electric variables
Pressure p_1	Voltage
Volume velocity U_1	Current
Inertance L	Series inductance
Viscous resistance R_{visc}	Series resistance
Compliance C	Capacitance to ground
Thermal-hysteresis resistance R_{therm}	Resistance to ground
Gain/loss along temperature gradient, G	Proportionally controlled current injector
Stroke-controlled transducer	Current source
Force-controlled transducer	Voltage source

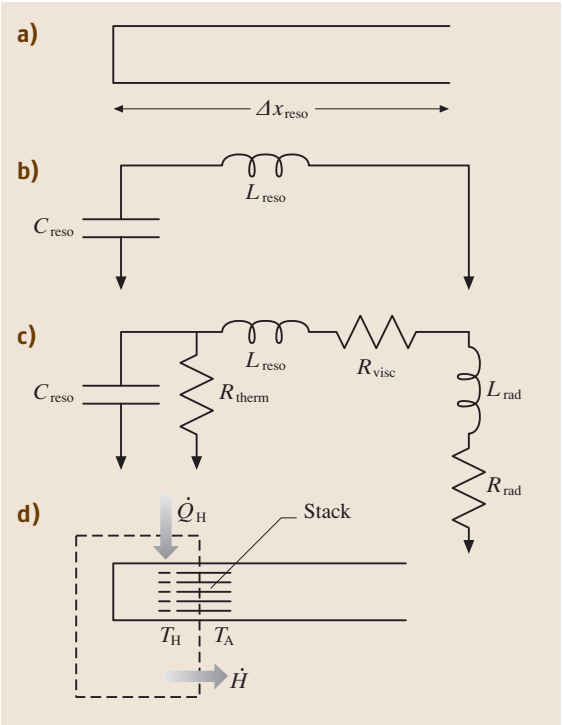

Fig. 7.1a–d Quarter-wavelength resonator. **(a)** A quarter-wavelength resonator: a tube closed at one end and open at the other. **(b)** A simple lossless lumped-element model of the resonator as a compliance C_{reso} in series with an inertance L_{reso}. **(c)** A more complicated lumped-element model, including thermal-hysteresis resistance R_{therm} in the compliance, viscous resistance R_{visc} in the inertance, and radiation impedance $R_{\mathrm{rad}} + \mathrm{i}\omega L_{\mathrm{rad}}$. **(d)** An illustration of the first law of thermodynamics for a control volume, shown enclosed by the dashed line, which intersects the stack of a well-insulated standing-wave engine. In steady state, the thermal power $\dot{Q}_{\mathrm{H}}$ that flows into the system at the hot heat exchanger must equal the total power $\dot{H}$ that flows along the stack

As introduced in Chap. 6 (Physical Acoustics) (7.3) is the acoustic Euler equation, the inviscid form of the momentum equation. It describes the force that the pressure gradient must exert to overcome the gas's inertia. In the lumped-element form (7.5), the geometrical and gas-property aspects of the inertia of the gas in the duct are represented by the duct's inertance L. Similarly introduced in Chap. 6, (7.4) and (7.6) are, respectively, the differential and lumped-element versions of the continuity equation combined with the gas's adiabatic equation of state. These describe the compressibility of the gas in response to being squeezed along the x-direction. In the lumped-element form (7.6), the geometrical and gas-property aspects of the compressibility of the gas in the duct are represented by the duct's compliance C.

Accurate calculation of the wave in a long duct or a long series of ducts requires analytical or numerical integration of differential equations [7.1], but for the purposes of this chapter we will consider lumped-element approximations, because they are satisfactorily accurate for many estimates, they allow a *circuit model* representation of devices, and they facilitate intuition based on experience with alternating-current (AC) electrical circuits. Table 7.1 shows the analogy between acoustic devices and electrical circuits.

For example, the closed–open resonator shown in Fig. 7.1a has a resonance frequency that can be calculated by setting its length Δx_{reso} equal to a quarter wavelength of sound; the result is $f_{\mathrm{reso}} = c/4\Delta x_{\mathrm{reso}}$. The simplest lumped-element approximation of the quarter-wavelength resonator is shown in Fig. 7.1b. We assign compliance C_{reso} to the left half of the resonator, because the compressibility of the gas is more important than its inertia in the left half, where $|p_1|$ is high and $|U_1|$ is low. Similarly, we assign inertance L_{reso} to the right half of the resonator, because the inertia is more important in the right half where $|U_1|$ is high. Setting $\Delta x = \Delta x_{\mathrm{reso}}/2$ in (7.7) and (7.8), and recalling that the resonance frequency of an electrical LC circuit is given by $\omega^2 = 1/LC$, we find $f_{\mathrm{reso}} = c/\pi\Delta x_{\mathrm{reso}}$, differing from the exact result only by a factor of $4/\pi$. Such accuracy will be acceptable for estimation and understanding in this chapter.

Circuit models can include as much detail as is necessary to convey the essential physics [7.1]. When the viscosity is included in the momentum equation, the lumped-element form becomes

$$\Delta p_1 = -\left(\mathrm{i}\omega L + R_{\mathrm{visc}}\right) U_1 \,, \tag{7.9}$$

and when the thermal conductivity and a temperature gradient in the x direction are included in the continuity equation, the lumped-element form becomes

$$\Delta U_1 = -\left(\mathrm{i}\omega C + \frac{1}{R_{\mathrm{therm}}}\right) p_1 + G U_{\mathrm{in},1} \,. \tag{7.10}$$

Figure 7.1c is a better model than Fig. 7.1b for the closed–open resonator of Fig. 7.1a, because it includes thermal-hysteresis resistance in the compliance, viscous resistance in the inertance, and the inertial and resistive radiation impedance at the open end. This model would yield reasonably accurate estimates for the free-decay time and quality factor of the resonator as well as its resonance frequency.

Ducts filled with porous media and having temperature gradients in the x-direction play a central role in thermoacoustic energy conversion [7.1]. The pore size is characterized by the hydraulic radius r_{h}, defined as the ratio of gas volume to gas–solid contact area. In a circular pore, r_{h} is half the circle's radius; in the gap between parallel plates, r_{h} is half the gap. The term *stack* is used for a porous medium whose r_{h} is comparable to the gas thermal penetration depth

$$\delta_{\mathrm{therm}} = \sqrt{2k/\omega\rho_{\mathrm{m}} c_{\mathrm{p}}} \,, \tag{7.11}$$

where k is the gas thermal conductivity and c_{p} is its isobaric heat capacity per unit mass, while a porous medium with $r_{\mathrm{h}} \ll \delta_{\mathrm{therm}}$ is known as a *regenerator*. The viscous penetration depth

$$\delta_{\mathrm{visc}} = \sqrt{2\mu/\omega\rho_{\mathrm{m}}} \,, \tag{7.12}$$

where μ is the viscosity, is typically comparable to, but smaller than, the thermal penetration depth. If the distance between a particular mass of gas and the nearest solid wall is much greater than the penetration depths, thermal and viscous interactions with the wall do not affect that gas.

In such porous media with axial temperature gradients, the gain/loss term $G U_{\mathrm{in},1}$ in (7.10) is responsible for the creation of acoustic power by engines and for the thermodynamically required consumption of acoustic power by refrigerators. This term represents cyclic thermal expansion and contraction of the gas as it moves along and experiences the temperature gradient in the solid. In regenerators, the gain G is nearly real, and ΔU_1 caused by the motion along the temperature gradient is in phase with U_1 itself, because of the excellent thermal contact between the gas in small pores and the

Table 7.2 Expressions for the lumped-element building blocks L, R_{visc}, C, R_{therm}, and $G U_1$, and for the total power $\dot{H}$, in the boundary-layer limit $r_{\mathrm{h}} \gg \delta$ and in the small-pore limit $r_{\mathrm{h}} \ll \delta$. The symbol "$\sim$" in the small-pore limit indicates that the numerical prefactor depends on the shape of the pore

	Boundary-layer limit	Small-pore limit
L	$\dfrac{\rho_{\mathrm{m}}\Delta x}{A}$	$\sim \dfrac{\rho_{\mathrm{m}}\Delta x}{A}$
R_{visc}	$\dfrac{\mu\Delta x}{A r_{\mathrm{h}}\delta_{\mathrm{visc}}}$	$\sim \dfrac{2\mu\Delta x}{A r_{\mathrm{h}}^2}$
C	$\dfrac{A\Delta x}{\rho_{\mathrm{m}} c^2} = \dfrac{A\Delta x}{\gamma p_{\mathrm{m}}}$	$\dfrac{\gamma A\Delta x}{\rho_{\mathrm{m}} c^2} = \dfrac{A\Delta x}{p_{\mathrm{m}}}$
R_{therm}	$\dfrac{\rho_{\mathrm{m}}^2 c_{\mathrm{p}}^2 T_{\mathrm{m}} r_{\mathrm{h}}\delta_{\mathrm{therm}}}{kA\Delta x}$	$\sim \dfrac{3kT_{\mathrm{m}}}{4\omega^2 r_{\mathrm{h}}^2 A\Delta x}$
$G U_1$	$\dfrac{1-\mathrm{i}}{2}\dfrac{1}{1+\sqrt{\sigma}}\dfrac{\delta_{\mathrm{therm}}}{r_{\mathrm{h}}}\dfrac{\Delta T_{\mathrm{m}}}{T_{\mathrm{m}}} U_1$	$\dfrac{\Delta T_{\mathrm{m}}}{T_{\mathrm{in,m}}} U_{\mathrm{in},1}$
$\dot{H}$	$\dfrac{\delta_{\mathrm{therm}}}{4r_{\mathrm{h}}(1+\sigma)} \mathrm{Re}\left\{\tilde{p}_1 U_1 \left[\mathrm{i}\left(1+\sqrt{\sigma}\right)+\left(1-\sqrt{\sigma}\right)\right]\right\}$ $-\dfrac{\delta_{\mathrm{therm}}\rho_{\mathrm{m}} c_{\mathrm{p}}\left(1-\sigma\sqrt{\sigma}\right)\lvert U_1\rvert^2}{4r_{\mathrm{h}} A\omega\left(1-\sigma^2\right)}\dfrac{\Delta T}{\Delta x}$ $+\dot{E} - \left(Ak + A_{\mathrm{solid}} k_{\mathrm{solid}}\right)\dfrac{\Delta T}{\Delta x}$	$-A_{\mathrm{solid}} k_{\mathrm{solid}}\dfrac{\Delta T}{\Delta x}$

walls of the pores. (Positive G indicates gain; negative G indicates loss.) In stacks, a nonzero imaginary part of G reflects imperfect thermal contact in the pores and the resultant time delay between the gas's cyclic motion along the solid's temperature gradient and the gas's thermal expansion and contraction.

Table 7.2 gives expressions for the impedances in the boundary-layer limit, $r_h \gg \delta_{therm}$ and $r_h \gg \delta_{visc}$, which is appropriate for large ducts, and in the small-pore limit appropriate for regenerators. Boundary-layer-limit entries are usefully accurate in stacks, in which $r_h \sim \delta$. General expressions for arbitrary r_h and many common pore shapes are given in [7.1].

The lumped-element approach summarized in Table 7.1 and the limiting expressions given in Table 7.2 are sufficient for most of this overview, but quantitatively accurate thermoacoustic analysis requires slightly more sophisticated techniques and includes more phenomena [7.1]. Every differential length dx of duct has dL, dC, dR_{visc}, and $d(1/R_{therm})$, and if $dT_m/dx \neq 0$ it also has dG, so a finite-length element is more analogous to an electrical transmission line than to a few lumped impedances. In addition to smoothly varying x dependencies for all variables, important phenomena include turbulence, which increases R_{visc} above the values given in Table 7.2; pore sizes which are in neither of the limits given in Table 7.2; nonlinear terms in the momentum and continuity equations, which cause frequency doubling, tripling, etc., so that the steady-state wave is a superposition of waves of many frequencies; and streaming flows caused by the wave itself. Many of these subjects are introduced in Chap. 8 (Nonlinear Acoustics). Thermoacoustics software that includes most or all of these phenomena and has the properties of several commonly used gases is available [7.19, 20].

For estimating the behavior of thermoacoustic devices, it is useful to remember some properties of common ideal gases [7.21]. The equation of state is

$$p = \frac{\rho R_{univ} T}{M} , \tag{7.13}$$

where $R_{univ} = 8.3\,\mathrm{J/(mole\,K)}$ is the universal gas constant and M is the molar mass. The ratio of isobaric to isochoric specific heats, γ, is 5/3 for monatomic gases such as helium and 7/5 for diatomic gases such as nitrogen and air near ambient temperature, and appears in both the adiabatic sound speed

$$c = \sqrt{\frac{\gamma R_{univ} T}{M}} \tag{7.14}$$

and the isobaric heat capacity per unit mass

$$c_p = \frac{\gamma R_{univ}}{(\gamma - 1)\, M} . \tag{7.15}$$

The viscosity of many common gases (e.g., air, helium, and argon) is about

$$\mu \simeq (2 \times 10^{-5}\,\mathrm{kg/m\,s}) \left(\frac{T}{300\,\mathrm{K}} \right)^{0.7} , \tag{7.16}$$

and the thermal conductivity k can be estimated by remembering that the Prandtl number

$$\sigma = \frac{\mu c_p}{k} \tag{7.17}$$

is about 2/3 for pure gases, but somewhat lower for gas mixtures [7.22].

7.2.2 Power

In addition to ordinary acoustic power $\dot{E}$, the time-averaged thermal power $\dot{Q}$, total power $\dot{H}$, and exergy flux $\dot{X}$ are important in thermoacoustic energy conversion. These thermoacoustic powers are related to the simpler concepts of work, heat, enthalpy, and exergy that are encountered in introductory [7.21] and advanced [7.23] thermodynamics.

Just as acoustic intensity is the time-averaged product of pressure and velocity, acoustic power $\dot{E}$ is the time-averaged product of pressure and volume velocity. In complex notation,

$$\dot{E} = \frac{1}{2} \mathrm{Re}\,(\tilde{p}_1 U_1) , \tag{7.18}$$

where the tilde denotes complex conjugation. At transducers, it is apparent that acoustic power is closely related to thermodynamic work, because a moving piston working against gas in an open space with volume V transforms mechanical power to acoustic power (or vice versa) at a rate $f \oint p\, dV$, which is equal to (7.18) for sinusoidal pressure and motion. Resistances R dissipate acoustic power; the gain/loss term GU_1 in components with temperature gradients can either consume or produce acoustic power, and inertances L and compliances C neither dissipate nor produce acoustic power, but simply pass it along while changing p_1 or U_1.

Time-averaged thermal power $\dot{Q}$ (i.e., time-averaged heat per unit time) is added to or removed from the gas at heat exchangers, which are typically arrays of tubes, high-conductivity fins, or both, spanning a duct. Thermal power can be supplied to an engine by high-temperature combustion products flowing through such

tubes or by circulation of a high-temperature heat-transfer fluid through such tubes and a source of heat elsewhere. Thermal power is often removed from engines and refrigerators by ambient-temperature water flowing through such tubes.

Of greatest importance is the total time-averaged power

$$\dot{H} = \int \left[\frac{1}{2} \rho_m \mathrm{Re}\left(\tilde{h}_1 u_1 \right) - k \frac{\mathrm{d}T_m}{\mathrm{d}x} \right] \mathrm{d}A \,, \qquad (7.19)$$

based on the x component u of velocity and the enthalpy h per unit mass, which is the energy of most utility in fluid mechanics. Fig. 7.1d uses a simple standing-wave engine (discussed more fully below) to illustrate the centrality of $\dot{H}$ to the first law of thermodynamics in thermoacoustics. The figure shows a heat exchanger and stack in a quarter-wavelength resonator. When heat is applied to the hot heat exchanger, the resonance is driven by processes (described below) in the stack. The dashed line in Fig. 7.1d encloses a volume whose energy must be constant when the engine is running in steady state. If the side walls of the engine are well insulated and rigid within that volume, then the only energy flows per unit time into and out of the volume are $\dot{Q}_H$ and whatever power flows to the right through the stack. We define the total power flow through the stack to be $\dot{H}$, and the first law of thermodynamics ensures that $\dot{H} = \dot{Q}_H$ in this simple engine.

As shown in (7.19), the total power $\dot{H}$ is the sum of ordinary steady-state heat conduction (most importantly in the solid parts of the stack or regenerator and the surrounding duct walls) and the total power carried convectively by the gas itself. Analysis of the gas contribution requires spatial and temporal averaging of the enthalpy transport in the gas [7.4], and shows that the most important contributions are acoustic power flowing through the pores of the stack and a shuttling of energy by the gas that occurs because entropy oscillations in the gas are nonzero and have a component in phase with velocity. Remarkably, these two phenomena nearly cancel in the small pores of a regenerator.

Finally, the exergy flux $\dot{X}$ represents the rate at which thermodynamic work can be done, in principle, with unrestricted access to a thermal bath at ambient temperature [7.1,23]. Exergy flux is sometimes used in complex systems to analyze sources of inefficiency according to location or process.

7.3 Engines

Implicit in Rayleigh's criterion [7.6] for spontaneous oscillations, "If heat be given to the air at the moment of greatest (density) or be taken from it at the moment of greatest rarefaction, the vibration is encouraged," is the existence of a vibration in need of encouragement, typically a resonance with a high quality factor. Today, we would express Rayleigh's criterion in either of two ways, depending on whether we adopt a Lagrangian perspective, focusing on discrete masses of gas as they move, or an Eulerian perspective, focusing on fixed locations in space as the gas moves past them. In the Lagrangian perspective, some of the gas in a thermoacoustic engine must experience $\oint p \, \mathrm{d}V > 0$, where V is the volume of an identified mass of gas. In the Eulerian perspective, part of the device must have $\mathrm{d}\dot{E}/\mathrm{d}x > 0$, arising from $\mathrm{Re}\,(\tilde{p}_1 \, \mathrm{d}U_1/\mathrm{d}x) > 0$ and the G term in (7.10).

By *engine* we mean a prime mover, i.e., something that converts heat to work or acoustic power. We describe three varieties: standing-wave engines, traveling-wave engines, and pulse combustors.

7.3.1 Standing-Wave Engines

Continuing the quarter-wavelength example introduced in Fig. 7.1, Fig. 7.2 shows a simple standing-wave engine, of a type that is available as a classroom demonstration [7.24]. A stack and hot heat exchanger are near the left end of the resonator, and its right end is open to the air. When heat $\dot{Q}_H$ is first applied to the hot heat exchanger, the heat exchanger and the adjacent end of the stack warm up, establishing an axial temperature gradient from hot to ambient in the stack. When the gradient is steep enough (as explained below), the acoustic oscillations start spontaneously, and grow in intensity as more heat is added and a steady state is approached. In the steady state, total power $\dot{H}$ equal to $\dot{Q}_H$ (minus any heat leak to the room) flows through the stack, creating acoustic power, some of which is dissipated elsewhere in the resonator and some of which is radiated into the room. To the right of the stack, where an ambient-temperature heat exchanger would often be located, the heat is carried rightward and out of this resonator by streaming-driven

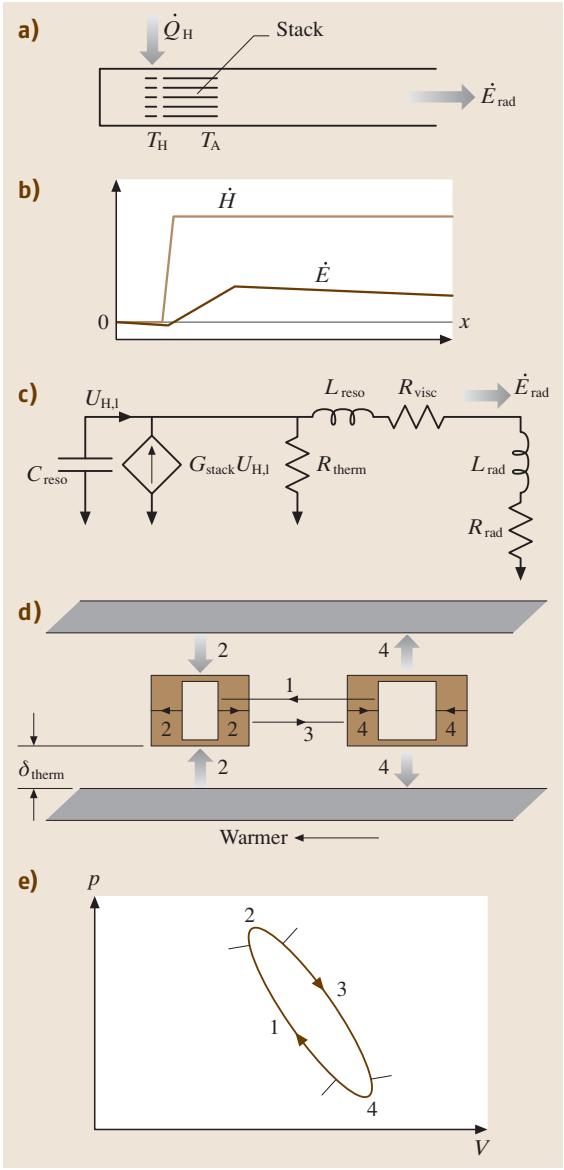

Fig. 7.2a–e A standing-wave engine. **(a)** A hot heat exchanger and a stack in a quarter-wavelength resonator. Heat $\dot{Q}_H$ is injected at the hot heat exchanger, and the device radiates acoustic power $\dot{E}_{rad}$ into the surroundings. **(b)** Total power flow $\dot{H}$ and acoustic power $\dot{E}$ as functions of position x in the device. Positive power flows in the positive-x direction. **(c)** Lumped-element model of the device. **(d)** Close-up view of part of one pore in the stack of **(a)**, showing a small mass of gas going through one full cycle, imagined as four discrete steps. *Thin arrows* represent motion, and *wide, open arrows* represent heat flow. **(e)** Plot showing how the pressure p and volume V of that small mass of gas evolve with time in a clockwise elliptical trajectory. *Tick marks* show approximate boundaries between the four numbered steps of the cycle shown in **(d)**

convection in the resonator, while fresh air at ambient temperature T_A streams inwards.

The most important process in the standing-wave engine is illustrated in Fig. 7.2d and Fig. 7.2e from a Lagrangian perspective. Figure 7.2d shows a greatly magnified view of a mass of gas inside one pore of the stack. The sinusoidal thermodynamic cycle of that mass of gas in pressure p and volume V is shown in Fig. 7.2e; the mass's temperature, entropy, density, and other properties also vary sinusoidally in time. However, for qualitative understanding of the processes, we describe the cycle as if it were a time series of four discrete steps, numbered 1–4 in Fig. 7.2d and Fig. 7.2e. In step 1, the gas is simultaneously compressed to a smaller volume and moved leftward by the wave a distance $2\,|\xi_1|$, which is much smaller than the length Δx of the stack. While the gas is moving leftwards, the pressure changes by $2\,|p_1|$ and the temperature would change by $2\,|T_1| = 2T_m(\gamma-1)\,|p_1|\,/\gamma p_m$ if the process were adiabatic. This suggests the definition of a critical temperature gradient

$$\nabla T_{crit} = |T_1|\,/\,|\xi_1| \ . \tag{7.20}$$

Thermal contact in the stack's large pores is imperfect, so step 1 is actually not too far from adiabatic. However, the temperature gradient imposed on the stack is greater than ∇T_{crit}, so the gas arrives at its new location less warm than the adjacent pore walls. Thus, in step 2, heat flows from the solid into the gas, warming the gas and causing thermal expansion of the gas to a larger volume. In step 3, the gas is simultaneously expanded to a larger volume and moved rightward by the wave. It arrives at its new location warmer than the adjacent solid, so in step 4 heat flows from the gas to the solid, cooling the gas and causing thermal contraction of the gas to a smaller volume. This brings it back to the start of the cycle, ready to repeat step 1.

Although the mass of gas under consideration returns to its starting conditions each cycle, its net effect on its surroundings is nonzero. First, its thermal expansion occurs at a higher pressure than its thermal contraction, so $\oint p\ \mathrm{d}V > 0$: the gas does work on its surroundings, satisfying Rayleigh's criterion. This work is responsible for the positive slope of $\dot{E}$ versus x in the stack in Fig. 7.2b and is represented by the gain element $G_{stack}U_{H,1}$ in

Fig. 7.2c. All masses of gas within the stack contribute to this production of acoustic power; one can think of the steady-state operation as due to all masses of gas within the stack adding energy to the oscillation every cycle, to make up for energy lost from the oscillation elsewhere, e.g., in viscous drag in the resonator and acoustic radiation to the surroundings. Second, the gas absorbs heat from the solid at the left extreme of its motion, at a relatively warm temperature, and delivers heat to the solid farther to the right at a lower temperature. In this way, all masses of gas within the stack pass heat along the solid, down the temperature gradient from left to right; within a single pore, the gas masses are like members of a bucket brigade (a line of people fighting a fire by passing buckets of water from a source of water to the fire while passing empty buckets back to the source). This transport of heat is responsible for most of $\dot{H}$ inside the stack, shown in Fig. 7.2b.

This style of engine is called *standing wave* because the time phasing between pressure and motion is close to that of a standing wave. (If it were *exactly* that of a standing wave, $\dot{E}$ would have to be exactly zero at all x.) To achieve the time phasing between pressure and volume changes that is necessary for $\oint p\ \mathrm{d}V > 0$, imperfect thermal contact between the gas and the solid in the stack is required, so that the gas can be somewhat thermally isolated from the solid during the motion in steps 1 and 3 but still exchange significant heat with the solid during steps 2 and 4. This imperfect thermal contact occurs because the distance between the gas and the nearest solid surface is of the order of δ_{therm}, and it causes R_{therm} to be significant, so standing-wave engines are inherently inefficient. Nevertheless, standing-wave engines are exceptionally simple. They include milliwatt classroom demonstrations like the illustration in Fig. 7.2, similar demonstrations with the addition of a water- or air-cooled heat exchanger at the ambient end of the stack, research engines [7.25, 26] up to several kW, and the Taconis and Sondhauss oscillations [7.5, 7]. Variants based on the same physics of intrinsically irreversible heat transfer include the *no-stack* standing-wave engine [7.27], which has two heat exchangers but no stack, and the Rijke tube [7.28], which has only a single, hot heat exchanger and uses a superposition of steady and oscillating flow of air through that heat exchanger to create $\oint p\ \mathrm{d}V > 0$.

7.3.2 Traveling-Wave Engines

One variety of what acousticians call traveling-wave engines has been known for almost two centuries as a Stirling engine [7.13, 29, 30], and is illustrated in Fig. 7.3a, Fig. 7.3b, Fig. 7.3f, and Fig. 7.3g. A regenerator bridges the gap between two heat exchangers, one at ambient temperature T_{A} and the other at hot temperature T_{H}; this assembly lies between two pistons, whose oscillations take the gas through a sinusoidal cycle that can be approximated as four discrete steps: compression, displacement rightward toward higher temperature, expansion, and displacement leftward toward lower temperature. For a small mass of gas in a single pore in the heart of the regenerator, the four steps of the cycle are illustrated in Fig. 7.3f. In step 1, the gas is compressed by rising pressure, rejecting heat to the nearby solid. In step 2, it is moved to the right, toward higher temperature, absorbing heat from the solid and experiencing thermal expansion as it moves. In step 3, the gas is expanded by falling pressure, and absorbs heat from the nearby solid. In step 4, the gas is moved leftward, toward lower temperature, rejecting heat to the solid and experiencing thermal contraction as it moves. The Stirling engine accomplishes $\oint p\ \mathrm{d}V > 0$ in Fig. 7.3g for each mass of gas in the regenerator, and this work production allows the hot piston to extract more work from the gas in each cycle than the ambient piston delivers to the gas.

The similarities and differences between this process and the standing-wave process of Fig. 7.2 are instructive. Here, the pore size is $\ll \delta_{\mathrm{therm}}$, so the thermal contact between the gas and the solid in the regenerator is excellent and the gas is always at the temperature of the part of the solid to which it is adjacent. Thus, the thermal expansion and contraction occur during the motion parts of the cycle, instead of during the stationary parts of the cycle in the standing-wave engine, and the pressure must be high during the rightward motion and low during the leftward motion to accomplish $\oint p\ \mathrm{d}V > 0$. This is the time phasing between motion and pressure that occurs in a traveling wave [7.14, 15], here traveling from left to right. The small pore size maintains thermodynamically reversible heat transfer, so R_{therm} is negligible, and traveling-wave engines have inherently higher efficiency than standing-wave engines. One remaining source of inefficiency is the viscous resistance R_{visc} in the regenerator, which can be significant because the small pores necessary for thermal efficiency cause R_{visc} to be large. To minimize the impact of R_{visc}, traveling-wave engines have $|p_1| > \rho_{\mathrm{m}} c\,|U_1|/A$, so the magnitude of the specific acoustic impedance $|z_{\mathrm{ac}}| = |p_1|\,A/|U_1|$ is greater than that of a traveling wave.

The gain G listed in Table 7.2 takes on a particularly simple form in the tight-pore limit: $G_{\mathrm{reg}} = \Delta T_{\mathrm{m}}/T_{\mathrm{in,m}}$.

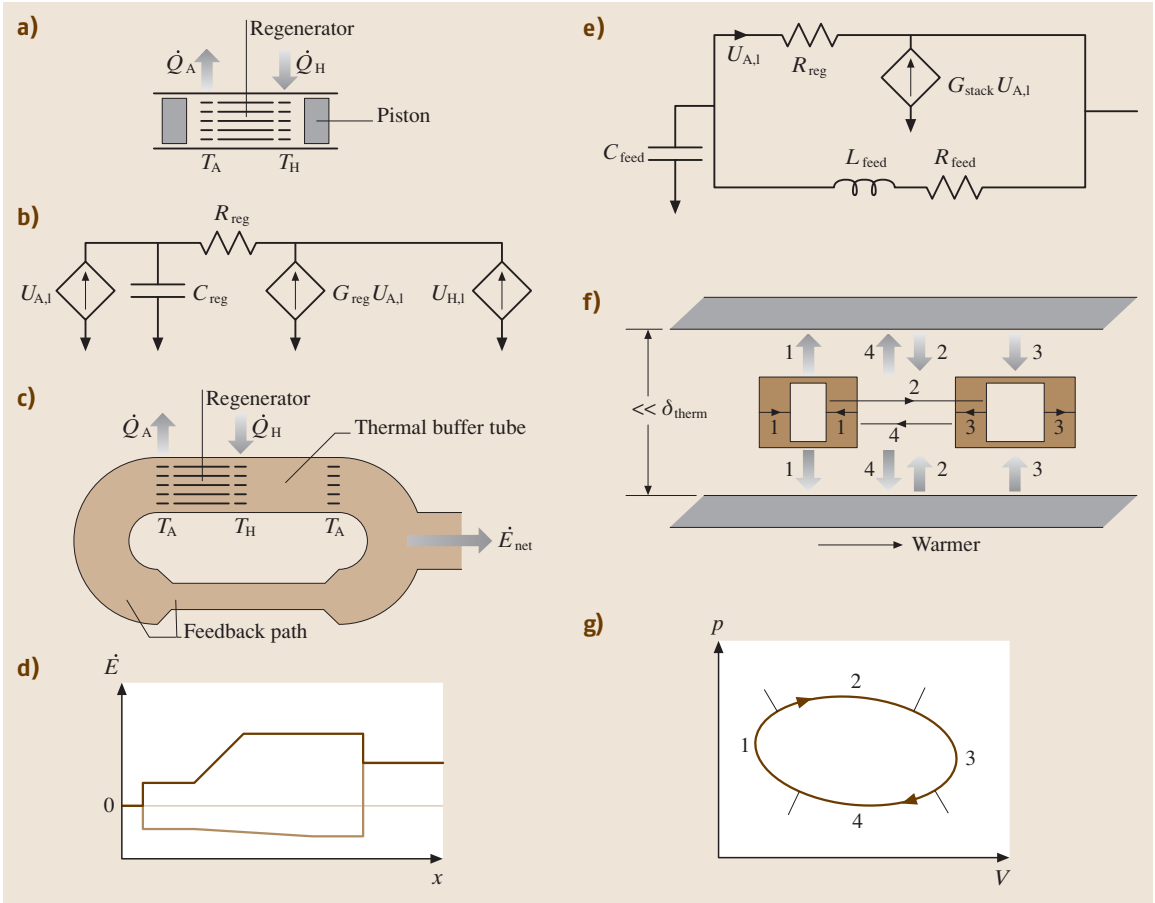

Fig. 7.3a–g Traveling-wave engines. **(a)** A Stirling engine. From *left to right*, the ambient piston, the ambient heat exchanger, the regenerator, the hot heat exchanger, and the hot piston. Time-averaged thermal power $\dot{Q}_H$ is injected into the gas at hot temperature T_H, waste thermal power $\dot{Q}_A$ is removed at ambient temperature T_A, and net mechanical power is extracted by the two pistons. **(b)** Lumped-element model of the engine in **(a)**. **(c)** Acoustic–Stirling hybrid engine, with the same processes as **(a)** in the regenerator and its two adjacent heat exchangers, but with additional acoustic components replacing the two pistons. **(d)** Acoustic power $\dot{E}$ as a function of position x in the device shown in **(c)**. Positive power flows in the positive-x direction, so the bottom branch of the curve represents power flowing leftward through the feedback path. Total power $\dot{H}$ is not shown, because it is essentially zero in the regenerator and essentially identical to $\dot{E}$ in the open parts of the device. **(e)** Lumped-element model of the engine in **(c)**. **(f)** Close-up view of part of one pore in the regenerator of **(a)** or **(c)**, showing a small mass of gas going through one full cycle, imagined as four discrete steps. **(g)** Plot showing how the pressure p and volume V of that small mass of gas evolve with time in a clockwise elliptical trajectory. *Tick marks* show approximate boundaries between the four steps of the cycle shown in **(f)**

In the engine of Fig. 7.3a, the initial temperature is T_A, and $\Delta T_m = T_H - T_A$, so the extra volume velocity that the lumped-element model injects at the right end of the regenerator is $U_{A,1}\,(T_H - T_A)\,/T_A$ and the total volume velocity at the right end of the regenerator is $U_{A,1}\,T_H/T_A$. Thus, the regenerator acts like an amplifier of volume velocity, with amplification T_H/T_A. If R_{reg} is small so that p_1 is nearly the same on both sides of the regenerator, then the regenerator amplifies $\dot{E}$ by nearly T_H/T_A.

Figure 7.3c-e illustrates a thermoacoustic–Stirling hybrid engine [7.16–18], in which the processes in the regenerator and its adjacent heat exchangers are the same

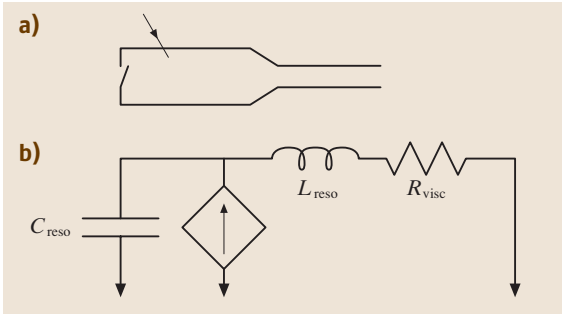

Fig. 7.4a,b Pulsed combustor. **(a)** From *left to right*, check valve for admitting fresh air, fuel injection, combustion cavity, neck. **(b)** Lumped-element model of the combustor

as in the Stirling engine and in Fig. 7.3f and Fig. 7.3g, but with acoustic elements replacing the Stirling engine's pistons. The toroidal topology of the thermoacoustic–Stirling hybrid allows some of the acoustic power that leaves the hot end of the regenerator to be fed back to the ambient end of the regenerator, eliminating the need for the Stirling engine's ambient piston. The feedback path has an inertance L_{feed} (with an unavoidable but small viscous resistance R_{feed}) and a compliance C_{feed}, with $1/L_{feed}C_{feed} \gg \omega^2$ and with ωL_{feed} significantly smaller than the regenerator viscous resistance R_{reg}. These choices let the $L_{feed}C_{feed}$ feedback path boost p_1 as acoustic power flows through it, providing the extra p_1 needed to drive U_1 into the regenerator at its ambient end.

The Stirling engine in Fig. 7.3a has a hot piston, which extracts acoustic power from the gas. From the hot piston's face, mechanical power flows from T_H to T_A along a temperature gradient in a moving part, either the piston itself or a connecting rod. In the thermoacoustic–Stirling hybrid engine of Fig. 7.3c, this thermal isolation function is accomplished by the thermal buffer tube, a thermally stratified column of moving gas. A well-designed thermal buffer tube passes acoustic power with little attenuation and has $\dot{H} \simeq \dot{E}$, so almost no thermal power flows from hot to ambient along the tube and little thermal power need be removed at the auxiliary heat exchanger at the thermal buffer tube's ambient end. Minimizing streaming and attendant heat convection in thermal buffer tubes, which otherwise causes $\dot{H} \neq \dot{E}$, is a topic of current research in thermoacoustics.

Traditional Stirling engines are used for propulsion in some submarines [7.31] and for auxiliary power in boats [7.32], and are under development for residential cogeneration of electricity and space heating [7.33], concentrated solar electricity generation, and nuclear generation of electricity for spacecraft [7.34]. In most of these applications, piston motion is converted to electricity via relative motion of wires and permanent magnets, either with a rotary alternator for crankshaft-coupled pistons or a linear alternator (reminiscent of a loudspeaker) for resonant *free-piston* configurations. Thermoacoustic-Stirling hybrid engines are under consideration for small-scale natural-gas liquefaction [7.25, 35] and for spacecraft power [7.36]. In the former case, acoustic power is fed directly from the engine to cryogenic acoustic refrigerators, without transduction to electrical power.

7.3.3 Combustion

In the standing-wave and traveling-wave engines, Rayleigh's criterion $\oint p \, dV > 0$ is met with volume changes that arise from temperature changes; those temperature changes, in turn, arise from thermal contact between the gas and nearby solid surfaces. In pulsed combustion, the volume changes needed to meet Rayleigh's criterion arise from both temperature and mole-number changes, which in turn are due to time-dependent chemical reactions whose rate is controlled by the time-dependent pressure or time-dependent velocity [7.37, 38].

Figure 7.4 illustrates one configuration in which pulsed combustion can occur. At the closed end of a closed–open resonator, a check valve periodically lets fresh air into the resonator and a fuel injector adds fuel, either steadily or periodically. If the rate of the exothermic chemical reaction increases with pressure (e.g., via the temperature's adiabatic dependence on pressure), positive dV occurs when p is high, meeting Rayleigh's criterion. A four-step diagram of the process, resembling Fig. 7.2d and Fig. 7.3f, is not included in Fig. 7.4 because the process is fundamentally not cyclic: a given mass of gas does not return to its starting conditions, but rather each mass of fresh-air–fuel mixture burns and expands only once.

Combustion instabilities can occur in rockets, jet engines, and gas turbines, with potentially devastating consequences if the pressure oscillations are high enough to cause structural damage. Much of the literature on thermoacoustic combustion is devoted to understanding such oscillations and using active or passive means to prevent them. However, some devices such as high-efficiency residential gas-fired furnaces deliberately use pulsed combustion as illustrated in Fig. 7.4 to pump fresh air in and exhaust gases out of the combus-

tor. This eliminates the need to leave the exhaust gases hot enough for strong chimney convection, so a larger fraction of the heat of combustion can be delivered to the home.

7.4 Dissipation

The dissipative processes represented above by R_{visc} and R_{therm} occur whenever gas-borne sound interacts with solid surfaces. Figure 7.5 illustrates this in the case of a short length dx of a large-radius duct with no axial temperature gradient. The origin of the viscous dissipation of acoustic power is viscous shear within the viscous penetration depth δ_{visc}, as shown in Fig. 7.5c. Most people find viscous dissipation intuitively plausible, imagining the frictional dissipation of mechanical energy when one surface rubs on another. More subtle is the thermal relaxation of acoustic power, illustrated in Fig. 7.5d and Fig. 7.5e. Gas is pressurized nearly adiabatically in step 1, then shrinks during thermal equilibration with the surface in step 2. It is depressurized nearly adiabatically in step 3, and then thermally expands during thermal equilibration with the surface during step 4. As shown in Fig. 7.5e, the net effect is $\oint p\ dV < 0$: the gas absorbs acoustic power from the wave, because the contraction occurs at high pressure and the expansion at low pressure. To avoid a hopelessly cluttered illustration, Fig. 7.5d shows the thermal-hysteresis process superimposed on the left–right oscillating motion in steps 1 and 3, but the thermal-hysteresis process occurs even in the absence of such motion.

Differentiating (7.18) with respect to x shows that the dissipation of acoustic power in the duct in length

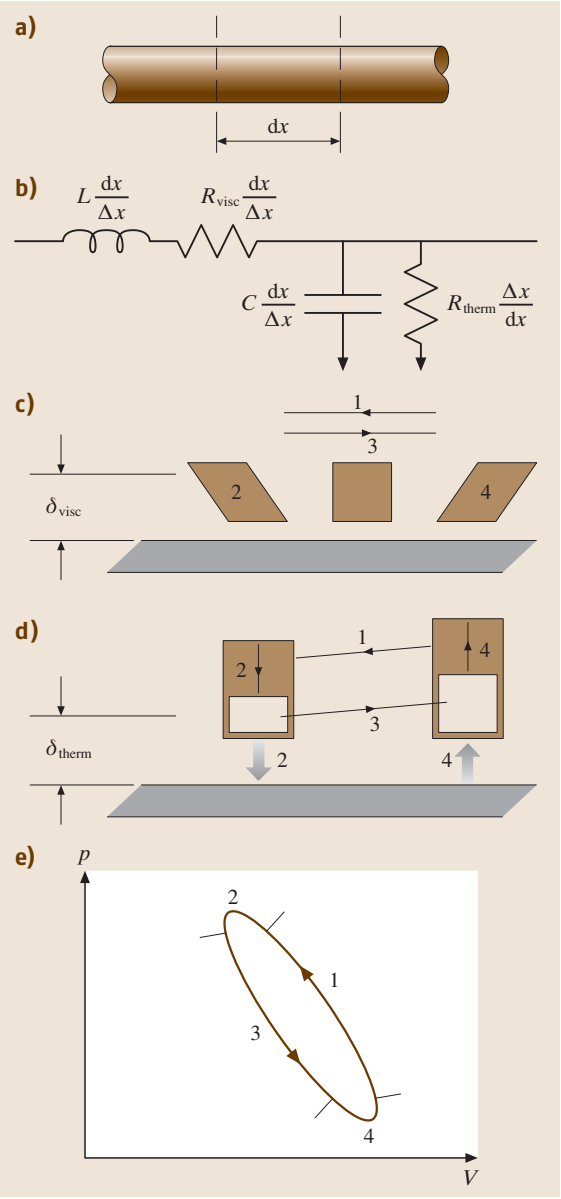

Fig. 7.5a–e Boundary dissipation in acoustic waves. **(a)** A duct with no temperature gradient, with one short length dx identified. **(b)** Each length dx has inertance, viscous resistance, compliance, and thermal hysteresis resistance. **(c)** The dissipation of acoustic power by viscous resistance is due to shear in the gas within roughly δ_{visc} of the boundary, here occurring during steps 1 and 3 of the cycle. **(d)** and **(e)** The dissipation of acoustic power by thermal relaxation hysteresis occurs within roughly δ_{therm} of the boundary. Gas is pressurized nearly adiabatically in step 1, then shrinks during thermal equilibration with the surface in step 2. It is depressurized nearly adiabatically in step 3, and then thermally expands during thermal equilibration with the surface during step 4. The net effect is that the gas absorbs acoustic power from the wave

$\mathrm{d}x$ is given by

$$\mathrm{d}\dot{E} = \frac{1}{2}\,\mathrm{Re}\left(\frac{\mathrm{d}\tilde{p}_1}{\mathrm{d}x}U_1 + \tilde{p}_1\frac{\mathrm{d}U_1}{\mathrm{d}x}\right)\,\mathrm{d}x\,, \tag{7.21}$$

and examination of (7.10) and (7.9) associates R_{visc} with the first term and R_{therm} with the second term. Expressions for R_{visc} and R_{therm} in the boundary-layer approximation are given in Table 7.2, and allow the expression of (7.21) in terms of the dissipation of acoustic power per unit of surface area S:

$$\mathrm{d}\dot{E} = \frac{1}{4}\rho_{\mathrm{m}}\,|u_1|^2\,\omega\delta_{\mathrm{visc}}\,\mathrm{d}S + \frac{1}{4}\,(\gamma-1)\,\frac{|p_1|^2}{\rho_{\mathrm{m}}c^2}\omega\delta_{\mathrm{therm}}\,\mathrm{d}S\,, \tag{7.22}$$

where $u_1 = U_1/A$ is the velocity outside the boundary layer, parallel to the surface. Each term in this result expresses a dissipation as the product of a stored energy per unit volume $\rho_{\mathrm{m}}\,|u_1|^2/4$ or $(\gamma-1)\,|p_1|^2/4\rho_{\mathrm{m}}c^2$, a volume $\delta_{\mathrm{visc}}\,\mathrm{d}S$ or $\delta_{\mathrm{therm}}\,\mathrm{d}S$, and a rate ω.

7.5 Refrigeration

7.5.1 Standing-Wave Refrigeration

The thermal-hysteresis process described in Sect. 7.4 consumes acoustic power without doing anything thermodynamically useful. Standing-wave refrigeration consumes acoustic power via a similar process, but achieves a thermodynamic purpose: pumping heat up a temperature gradient, either to remove heat from a temperature below ambient or (less commonly) to deliver heat to a temperature above ambient. Figure 7.6a–c shows a standing-wave refrigerator of the style pioneered by *Hofler* [7.8, 9] and recently studied by *Tijani* [7.39]. At the left end, a driver such as a loudspeaker injects acoustic power $\dot{E}$, which flows rightward through the stack, causing a leftward flow of total energy $\dot{H}$.

The most important process in a standing-wave refrigerator is illustrated in Fig. 7.6d and Fig. 7.6e from a Lagrangian perspective. Fig. 7.6d shows a greatly magnified view of a small mass of gas inside one pore of the stack. The sinusoidal thermodynamic cycle of that mass of gas in pressure p and volume V is shown in Fig. 7.6e; the mass's temperature, entropy, density, and other properties also vary sinusoidally in time. However, for qualitative understanding of the processes, we describe them as if they are a time series of four discrete steps, numbered 1–4 in Fig. 7.6d and Fig. 7.6e. In step 1, the gas is simultaneously compressed to a smaller volume and moved leftward by the wave. Thermal contact is imperfect in the pores of a stack, so during step 1 the gas experiences a nearly adiabatic temperature increase due to the pressure increase that causes the compression. It arrives at its new location warmer than the adjacent solid because the temperature gradient in the solid is less than the critical temperature gradient ∇T_{crit} defined in (7.20). Thus, in step 2, heat flows from the gas into the solid, cooling the gas and causing thermal contraction of the gas to a smaller volume. In step 3, the gas is simultaneously expanded to a larger volume and moved rightward by the wave. It arrives at its new location cooler than the adjacent solid, so in step 4 heat flows from the solid to the gas, warming the gas and causing thermal expansion of the gas to a larger volume. This brings it back to the start of the cycle, ready to repeat step 1.

The mass of gas shown in Fig. 7.6d has two time-averaged effects on its surroundings. First, the gas absorbs heat from the solid at the right extreme of its motion, at a relatively cool temperature, and delivers heat to the solid farther to the left at a higher temperature. In this way, all masses of gas within the stack pass heat along the solid, up the temperature gradient from right to left—within a single pore, the gas masses are like members of a bucket brigade passing water. This provides the desired refrigeration or heat-pumping effect. If the left heat exchanger is held at ambient temperature, as shown in Fig. 7.6a, then the system is a refrigerator, absorbing thermal power $\dot{Q}_{\mathrm{C}}$ from an external load at the right heat exchanger at one end of the bucket brigade at T_{C}, as waste thermal power is rejected to an external ambient heat sink at the other end of the bucket brigade at T_{A}. (The system functions as a heat pump if the right heat exchanger is held at ambient temperature; then the left heat exchanger is above ambient temperature.) Second, the gas's thermal expansion occurs at a lower pressure than its thermal contraction, so $\oint p\,\mathrm{d}V < 0$: the gas absorbs work from its surroundings. This work is responsible for the negative slope of $\dot{E}$ versus x in the stack in Fig. 7.6b and is represented by the gain element $G_{\mathrm{stack}}U_{\mathrm{A},1}$ in Fig. 7.6c. All masses of gas within the stack contribute

to this consumption of acoustic power, which must be supplied by the driver.

As in the standing-wave engine, the time phasing between pressure and motion in the standing-wave refrigerator is close to that of a standing wave. Imperfect thermal contact between the gas and the solid in the stack is required to keep the gas rather isolated from the solid during the motion in steps 1 and 3 but still able to exchange significant heat with the solid during steps 2 and 4. This imperfect thermal contact occurs because the distance between the gas and the nearest solid surface is of the order of δ_{therm}, and it causes R_{therm} to be significant, so standing-wave refrigerators are inherently inefficient.

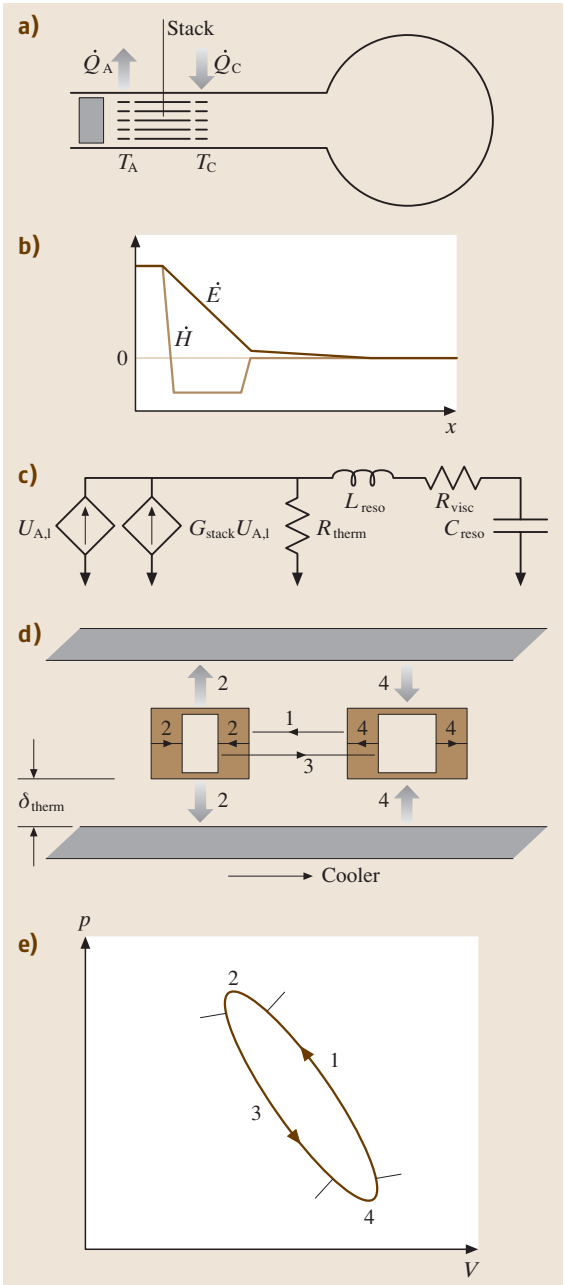

Fig. 7.6a–e A standing-wave refrigerator. **(a)** From *left to right*, a piston, ambient heat exchanger, stack, cold heat exchanger, tube, and tank. Acoustic power is supplied to the gas by the piston to maintain the standing wave, and results in thermal power $\dot{Q}_C$ being absorbed by the gas from a load at cold temperature T_C while waste thermal power $\dot{Q}_A$ is rejected by the gas to an external heat sink at ambient temperature T_A. **(b)** Total power flow $\dot{H}$ and acoustic power $\dot{E}$ as functions of position x in the device. Positive power flows in the positive-x direction. **(c)** Lumped-element model of the device. **(d)** Close-up view of part of one pore in the stack of **(a)**, showing a small mass of gas going through one full cycle, imagined as four discrete steps. **(e)** Plot showing how the pressure p and volume V of that small mass of gas evolve with time in a counter-clockwise elliptical trajectory. *Tick marks* show approximate boundaries between the four steps of the cycle shown in **(d)**

7.5.2 Traveling-Wave Refrigeration

Several varieties of traveling-wave refrigerator are commercially available or under development. At their core is a regenerator, in which the process shown in Fig. 7.7a,b operates. In step 1 of the process, the gas is compressed by rising pressure, rejecting heat to the nearby solid. In step 2, it is moved to the right, toward lower temperature, rejecting heat to the solid and experiencing thermal contraction as it moves. In step 3, the gas is expanded by falling pressure, and absorbs heat from the nearby solid. In step 4, the gas is moved leftward, toward higher temperature, absorbing heat from the solid and experiencing thermal expansion as it moves. The heat transfers between gas and solid in steps 2 and 4 are equal and opposite, so the net thermal effect of each mass of gas on the solid is due to steps 1 and 3, and is to move heat from right to left, up the temperature gradient. As before, the motion of any particular mass of gas is less than the length of the regenerator, so the heat is passed bucket-brigade fashion from the cold end of the regenerator to the ambient end. Each mass of gas absorbs $\oint p\, dV$ of acoustic power from the wave as shown in Fig. 7.7b, because the thermal contraction in step 2 occurs at high pres-

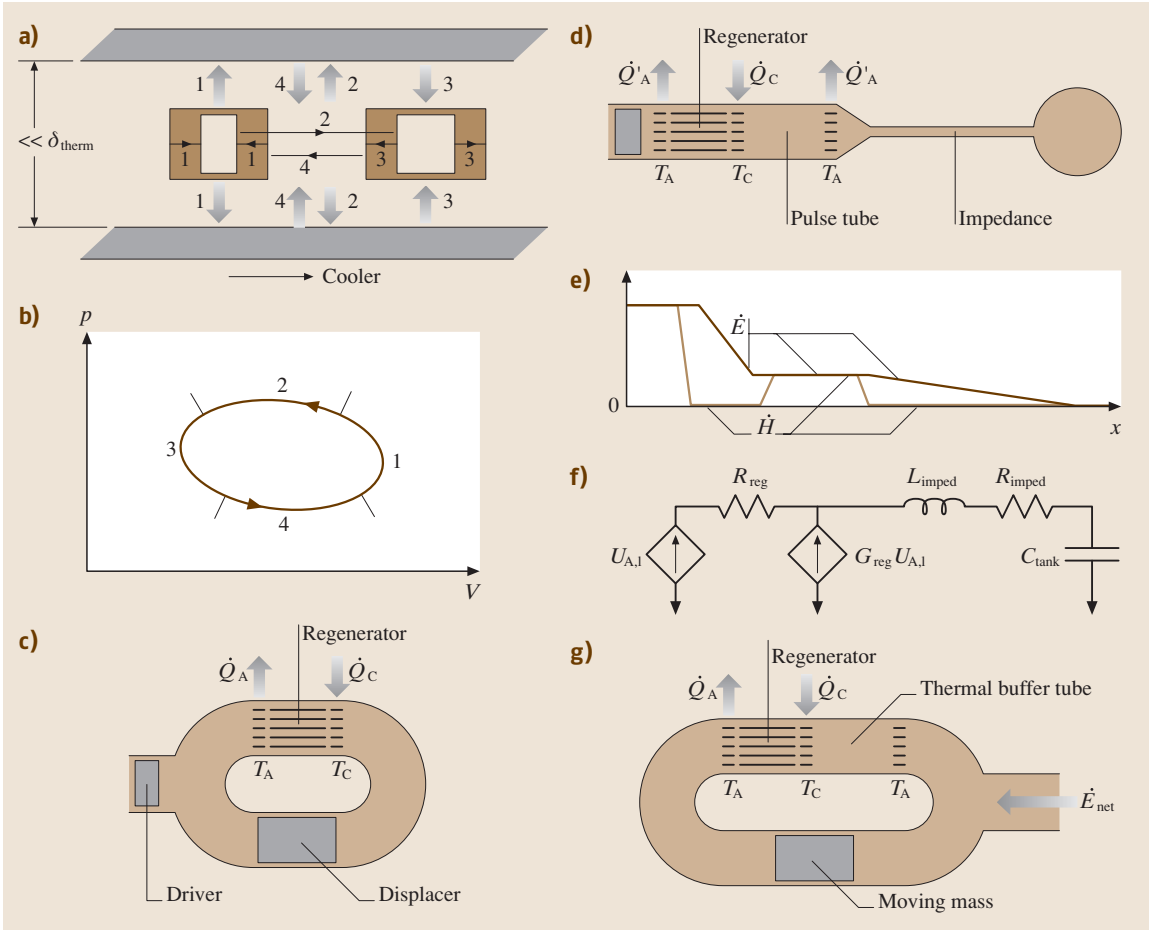

Fig. 7.7a–g Traveling-wave refrigerators. **(a)** Close-up view of part of one pore in the regenerator of a traveling-wave refrigerator, showing a small mass of gas going through one full cycle, imagined as four discrete steps. **(b)** Plot showing how the pressure p and volume V of that small mass of gas evolve with time in a counterclockwise elliptical trajectory. Tick marks show approximate boundaries between the four steps of the cycle shown in **(a)**. **(c)** A traditional Stirling refrigerator. From *left to right*, the ambient driver piston; the ambient heat exchanger, the regenerator, and the cold heat exchanger are across the top; the displacer is below. Time-averaged thermal power $\dot{Q}_C$ is removed by the gas from an external heat load at cold temperature T_C, while waste thermal power $\dot{Q}_A$ is rejected by the gas to an external heat sink at ambient temperature T_A and net acoustic power is supplied to the gas by the driver. **(d)** Pulse-tube refrigerator, with the same processes as **(c)** in the regenerator and its two adjacent heat exchangers, but with the displacer replaced by acoustic components. **(e)** Acoustic power $\dot{E}$ and total power $\dot{H}$ as functions of position x in the device shown in **(d)**. Positive power flows in the positive-x direction. **(f)** Lumped-element model of the pulse-tube refrigerator in **(d)**. **(g)** A refrigerator in which the thermal-buffer function and moving-mass function of **(c)**'s displacer are in two separate components

sure and the thermal expansion in step 4 occurs at low pressure. The small pore size, $r_h \ll \delta_{therm}$, maintains thermodynamically reversible heat transfer, so R_{therm} is negligible, and traveling-wave refrigerators have an inherently high efficiency. Acoustically, the process shown in Fig. 7.7a represents acoustic power traveling from left to right through the regenerator, and being partly consumed as it goes. Different varieties of traveling-wave refrigerator use different methods to create the necessary amplitudes and relative time phasing of motion and pressure to achieve this acoustic power flow through the regenerator.

The traditional Stirling refrigerator [7.40] uses two moving pistons, which can be either crankshaft-coupled in a configuration like that of the engine in Fig. 7.3a or of the *free-displacer* variety shown in Fig. 7.7c. In the free-displacer Stirling refrigerator (often called *free piston*), the solid displacer moves in response to the gas-pressure forces on it, without linkage to any external motor. Its area and mass are selected to give its motion the desired amplitude and time phase [7.29]. Acoustic power is transmitted through it, from right to left, so that the acoustic power that flows out of the right end of the regenerator is fed through the displacer to the left, added to the acoustic power supplied by the driver, and injected into the left end of the regenerator. The displacer must be a thermal insulator, because its right end is at T_C and its left end at T_A. Crankshaft-coupled Stirling refrigerators were used in the 19th century to keep beef cold on the long sea voyage from South America to Britain. Free-piston Stirling cryocoolers are in common use today for cooling infrared sensors in military night-vision goggles and surveillance satellites, and a free-piston Stirling refrigerator built into a small, portable *ice chest* is commercially available at low cost for picnics [7.41].

The pulse-tube refrigerator [7.12], illustrated in Fig. 7.7d–f, uses only one piston. The acoustic power flowing out of the right end of the regenerator is absorbed in an acoustic impedance, instead of being fed back to the left end of the regenerator. This gives the pulse-tube refrigerator a lower efficiency than the Stirling refrigerator, but for cryogenic applications the reduced efficiency is a small price to pay for the elimination of the Stirling's cold moving part. The lumped-element model of the impedance and adjacent tank shown in Fig. 7.7f correctly suggests that proper design of L_{imped}, R_{imped}, and C_{tank} can create almost any desired ratio of $|U_1|$ to $|p_1|$ and time phasing between U_1 and p_1 at the right end of the regenerator. The desired impedance is often achieved by choosing $R_{\text{visc}} \sim \omega L_{\text{imped}} \gg 1/\omega C_{\text{imped}}$. The so-called pulse tube, and the ambient heat exchanger to its right, thermally isolate the cold heat exchanger from the dissipation of acoustic power in the impedance, just as the thermal buffer tube performs that function in Fig. 7.3c. Pulse-tube refrigerators are in common use today in satellites [7.42] and are under development for many other applications such as small-scale oxygen liquefaction and cooling superconducting equipment.

Another variation of the theme is shown in Fig. 7.7g, where the thermal buffer tube and the moving mass perform the thermal-insulation and inertial functions of the free displacer of Fig. 7.7c in two separate locations [7.43,44]. This variety is under development for commercial food refrigeration [7.45]. Yet another variety [7.46] replaces the inertial moving mass of Fig. 7.7g with inertial moving gas, similar to the thermoacoustic–Stirling hybrid engine of Fig. 7.3c.

7.6 Mixture Separation

In thermoacoustic mixture separation, acoustic power causes the components of a gas mixture to separate [7.47, 48]. The process is loosely analogous to the pumping of heat through the stack in a standing-wave refrigerator. The expenditure of acoustic power results in an increase in the Gibbs free energy of the mixture's components, and the efficiency of the process is comparable to that of some other practical separation processes [7.49].

Figure 7.8 illustrates the process for a binary gas mixture of heavy and light molecules, whose motions are indicated by filled and open arrows, respectively. The motion of the molecules in steps 1 and 3 of the process is bulk motion of the gas, and the motion during steps 2 and 4 is thermal diffusion, in which light molecules diffuse toward higher temperature and heavy molecules diffuse toward lower temperature. In step 1, the gas in the center of the pore moves leftward and its pressure rises, so its temperature rises nearly adiabatically. Trapped by the viscous boundary layer near the wall of the tube is some other gas that does not move and whose thermal contact with the pore wall keeps its temperature from rising. During step 2, the temperature difference between the central gas and the peripheral gas causes light atoms to diffuse into the center and heavy atoms to diffuse out of the center, enriching the center in light atoms. Bulk motion rightward in step 3 carries this central light-enriched gas to the right. Simultaneously, the pressure drops in step 3, and hence the central temperature drops nearly adiabatically. Thus thermal diffusion in step 4 pulls heavy molecules into the center and drives light molecules out of the center, leaving the center enriched in heavy molecules so that the leftward motion during step 1 carries heavy-enriched gas leftward. The net effect of steps 1 and 3 is to move heavy molecules leftward and light molecules rightward. The process

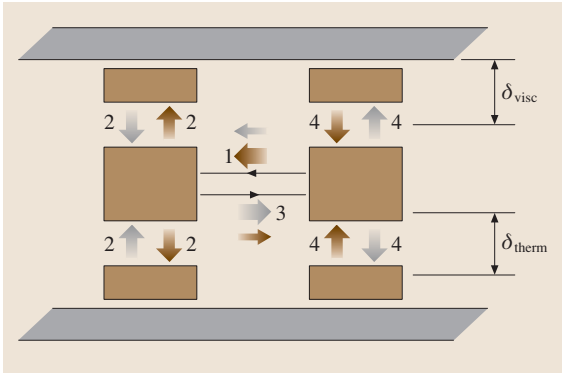

Fig. 7.8 Close-up view of part of one pore in a thermoacoustic mixture separator, showing a small body of gas in the center of the pore going through one full cycle, imagined as four discrete steps, and exchanging mass with neighboring, immobile gas. The *gray* and *brown arrows* in steps 2 and 4 signify thermally driven diffusion of light and heavy molecules between the central gas and the peripheral gas close to the wall of the pore. In steps 1 and 3, the *gray* and *brown arrows* signify bulk motion of the gas, without diffusion

takes place when the mole-fraction gradient is less than a critical gradient, analogous to the critical temperature gradient below which standing-wave refrigeration occurs.

As is evident from Fig. 7.8, the process works best for tubes with r_h somewhat larger than δ_{therm} and δ_{visc}. However, unlike the description above, the process actually works best near traveling-wave phasing, because two 45° phase shifts were ignored in that description. High separation purities require long tubes, and high mole fluxes will require many passages in parallel, perhaps in structures similar to the stacks of standing-wave engines and refrigerators.

In a 2 m-long tube, a 50–50 helium–argon mixture has been separated to yield 70% helium, 30% argon at one end and 30% helium, 70% argon at the other end; and a measurable enrichment of ^{22}Ne from natural neon has been achieved [7.50].

References

7.1 G.W. Swift: *Thermoacoustics: A Unifying Perspective for some Engines and Refrigerators* (Acoustical Society of America Publications, Sewickley PA 2002)

7.2 S.L. Garrett: Resource letter TA-1, Thermoacoustic engines and refrigerators, Am. J. Phys. **72**, 11–17 (2004)

7.3 N. Rott: Damped and thermally driven acoustic oscillations in wide and narrow tubes, Z. Angew. Math. Phys. **20**, 230–243 (1969)

7.4 N. Rott: Thermally driven acoustic oscillations, Part III: Second-order heat flux, Z. Angew. Math. Phys. **26**, 43–49 (1975)

7.5 T. Yazaki, A. Tominaga, Y. Narahara: Experiments on thermally driven acoustic oscillations of gaseous helium, J. Low Temp. Phys. **41**, 45–60 (1980)

7.6 J.W. Strutt (Baron Rayleigh): The explanation of certain acoustical phenomena, Nature **18**, 319–321 (1878)

7.7 K.T. Feldman: Review of the literature on Sondhauss thermoacoustic phenomena, J. Sound Vibrat. **7**, 71–82 (1968)

7.8 T. Hofler, J.C. Wheatley, G.W. Swift, A. Migliori: Acoustic cooling engine, US Patent No. 4,722,201. (1988)

7.9 T.J. Hofler: *Thermoacoustic refrigerator design and performance. Ph.D. thesis, Physics Department* (University of California, San Diego 1986)

7.10 W.E. Gifford, R.C. Longsworth: Pulse tube refrigeration progress, Adv. Cryogenic Eng. B **10**, 69–79 (1965)

7.11 E.L. Mikulin, A.A. Tarasov, M.P. Shkrebyonock: Low-temperature expansion pulse tubes, Adv. Cryogenic Eng. **29**, 629–637 (1984)

7.12 R. Radebaugh: *Development of the pulse tube refrigerator as an efficient and reliable cryocooler* (Proc. Inst. Refrigeration, London 2000) pp. 11–29

7.13 G. Walker: *Stirling Engines* (Clarendon, Oxford 1960)

7.14 P.H. Ceperley: A pistonless Stirling engine – The traveling wave heat engine, J. Acoust. Soc. Am. **66**, 1508–1513 (1979)

7.15 P.H. Ceperley: Gain and efficiency of a short traveling wave heat engine, J. Acoust. Soc. Am. **77**, 1239–1244 (1985)

7.16 T. Yazaki, A. Iwata, T. Maekawa, A. Tominaga: Traveling wave thermoacoustic engine in a looped tube, Phys. Rev. Lett. **81**, 3128–3131 (1998)

7.17 C.M. de Blok: Thermoacoustic system, 1998. Dutch Patent: International Application Number PCT/NL98/00515. US Patent 6,314,740, November 13 (2001)

7.18 S. Backhaus, G.W. Swift: A thermoacoustic-Stirling heat engine, Nature **399**, 335–338 (1999)

7.19 D. Gedeon: *A globally implicit Stirling cycle simulation, Proceedings of the 21st Intersociety Energy Conversion Engineering Conference* (Am. Chem. Soc.,

Washington 1986) pp. 550–554, Software available from Gedeon Associates, Athens, Ohio
7.20 W.C. Ward, G.W. Swift: Design environment for low amplitude thermoacoustic engines (DeltaE), J. Acoust. Soc. Am. **95**, 3671–3672 (1994), Software and user's guide available either from the Los Alamos thermoacoustics web site www.lanl.gov/thermoacoustics/ or from the Energy Science and Technology Software Center, US Department of Energy, Oak Ridge, Tennessee
7.21 R.E. Sonntag, C. Borgnakke, G.J. Van Wylen: *Fundamentals of Thermodynamics* (Wiley, New York 2003)
7.22 F.W. Giacobbe: Estimation of Prandtl numbers in binary mixtures of helium and other noble gases, J. Acoust. Soc. Am. **96**, 3568–3580 (1994)
7.23 A. Bejan: *Advanced Engineering Thermodynamics*, 2nd edn. (Wiley, New York 1997)
7.24 Acoustic Laser Kit, Graduate Program in Acoustics, P. O. Box 30, State College, PA 16804-0030 (www.acs.psu.edu/thermoacoustics/refrigeration/laserdemo.htm)
7.25 G.W. Swift, J.J. Wollan: Thermoacoustics for liquefaction of natural gas, GasTIPS **8**(4), 21–26 (2002), Also available at www.lanl.gov/thermoacoustics/Pubs/GasTIPS.pdf
7.26 D.L. Gardner, G.W. Swift: A cascade thermoacoustic engine, J. Acoust. Soc. Am. **114**, 1905–1919 (2003)
7.27 R.S. Wakeland, R.M. Keolian: Thermoacoustics with idealized heat exchangers and no stack, J. Acoust. Soc. Am. **111**, 2654–2664 (2002)
7.28 K.T. Feldman: Review of the literature on Rijke thermoacoustic phenomena, J. Sound Vibrat. **7**, 83–89 (1968)
7.29 I. Urieli, D.M. Berchowitz: *Stirling Cycle Engine Analysis* (Adam Hilger, Bristol 1984)
7.30 A.J. Organ: *Thermodynamics and Gas Dynamics of the Stirling Cycle Machine* (Cambridge Univ. Press, Cambridge 1992)
7.31 H. Nilsson, C. Bratt: Test results from a 15 kW air-independent Stirling power generator. In: *Proc. 6th International Symposium on Unmanned Untethered Submersible Technology* (IEEE, 1989) pp. 123–128
7.32 WhisperGen Limited, Christchurch, New Zealand
7.33 S. Qiu, D.L. Redinger, J.E. Augenblick: The next generation infinia free-piston Stirling engine for micro-CHP applications. In: *Proc. 12th International Stirling Engine Conference* (Durham University, 2005) pp. 156–165
7.34 M.A. White: A new paradigm for high-power Stirling applications, Proc. Space Nuclear Conference, Stirling Technology Company, Kennewick WA (2005)
7.35 B. Arman, J. Wollan, V. Kotsubo, S. Backhaus, G. Swift: Operation of thermoacoustic Stirling heat engine driven large multiple pulse tube refrigerators. In: *Cryocoolers 13*, ed. by R.G. Ross (Springer, Berlin, New York 2005) pp. 181–188
7.36 S. Backhaus, E. Tward, M. Petach: Traveling-wave thermoacoustic electric generator, Appl. Phys. Lett. **85**, 1085–1087 (2004)
7.37 B. Zinn: Pulsating combustion. In: *Advanced Combustion Methods*, ed. by F.J. Weinberg (Academic, London 1986) pp. 113–181
7.38 F.E.C. Culick: Combustion instabilities and Rayleigh's criterion. In: *Modern Research Topics in Aerospace Propulsion*, ed. by C. Casci, G. Angelino, L. DeLuca, W.A. Sirignano (Springer, Berlin, New York 1991) pp. 508–517, (in honor of Corrado Casci)
7.39 M.E.H. Tijani, J.C.H. Zeegers, A.T.A.M. deWaele: The optimal stack spacing for thermoacoustic refrigeration, J. Acoust. Soc. Am. **112**, 128–133 (2002)
7.40 G. Walker: *Cryocoolers* (Plenum, New York 1983)
7.41 N.W. Lane: Commercialization status of free-piston Stirling machines. In: *Proc. 12th International Stirling Engine Conference* (Durham University, 2005) pp. 30–37
7.42 E. Tward, C.K. Chan, C. Jaco, J. Godden, J. Chapsky, P. Clancy: Miniature space pulse tube cryocoolers, Cryogenics **39**, 717–720 (1999)
7.43 R.W.M. Smith, M.E. Poese, S.L. Garrett, R.S. Wakeland: Thermoacoustic device, US Patent No. 6,725,670.(2004)
7.44 M. E. Poese, R. W. M. Smith, R. S. Wakeland, S. L. Garrett: Bellows bounce thermoacoustic device, US Patent No. 6,792,764.(2004)
7.45 S.L. Garret: Pennsylvania State University, private communication
7.46 G.W. Swift, D.L. Gardner, S. Backhaus: Acoustic recovery of lost power in pulse tube refrigerators, J. Acoust. Soc. Am. **105**, 711–724 (1999)
7.47 D.A. Geller, G.W. Swift: Saturation of thermoacoustic mixture separation, J. Acoust. Soc. Am. **111**, 1675–1684 (2002)
7.48 P.S. Spoor, G.W. Swift: Thermoacoustic separation of a He-Ar mixture, Phys. Rev. Lett. **85**, 1646–1649 (2000)
7.49 D.A. Geller, G.W. Swift: Thermodynamic efficiency of thermoacoustic mixture separation, J. Acoust. Soc. Am. **112**, 504–510 (2002)
7.50 D.A. Geller, G.W. Swift: Thermoacoustic enrichment of the isotopes of neon, J. Acoust. Soc. Am. **115**, 2059–2070 (2004),